The External Limiting Membrane in Early-Onset Stargardt Disease

Winston Lee,[1] Kalev Nõupuu,[1,2] Maris Oll,[1,2] Tobias Duncker,[1] Tomas Burke,[3] Jana Zernant,[1] Srilaxmi Bearelly,[1] Stephen H. Tsang,[1,4] Janet R. Sparrow,[1,4] and Rando Allikmets[1,4]

[1]Department of Ophthalmology, Columbia University, New York, New York, United States
[2]Eye Clinic, Tartu University Hospital, Tartu, Estonia
[3]Department of Ophthalmology, Royal United Hospital, Bath, United Kingdom
[4]Department of Pathology & Cell Biology, Columbia University, New York, New York, United States

PURPOSE. To describe pathologic changes of the external limiting membrane (ELM) in young patients with early-onset Stargardt (STGD1) disease.

METHODS. Twenty-six STGD1 patients aged younger than 20 years with confirmed disease-causing adenosine triphosphate–binding cassette, subfamily A, member 4 (ABCA4) alleles and 30 age-matched unaffected individuals were studied. Spectral-domain optical coherence tomography (SD-OCT), fundus autofluorescence (AF), and color fundus photography (CFP) images, as well as full-field electroretinograms were obtained and analyzed for one to four visits in each patient.

RESULTS. The ELM in all patients exhibited a distinct thickening that was not observed in unaffected individuals. In addition, accumulations of reflective deposits were noted in the outer nuclear layer in every patient. Four patients exhibited a concave protuberance or bulging of a thickened and hyperreflective ELM band within the fovea containing preserved photoreceptors. Longitudinal SD-OCT data in several patients revealed the persistence of this ELM abnormality over a period of time (1–4 years). Furthermore, the edges of the inner segment ellipsoid band appeared to recede earlier than the ELM band in active lesions.

CONCLUSIONS. Structural changes seen in the ELM of this cohort may reflect a gliotic response to cellular stress at the photoreceptor level in early-onset STGD1.

Keywords: Stargardt disease, ABCA4, external limiting membrane, Müller cell, photoreceptor

Stargardt disease (STGD1; OMIM #248200) is an autosomal recessive juvenile macular dystrophy affecting between 1 in 8000 and 1 in 10,000 people worldwide.[1,2] It is caused by more than 800 disease-causing mutations in the *ABCA4* gene, which encodes for the photoreceptor-specific ATP-binding cassette transporter.[3] A dysfunctional ABCA4 protein results in inadequate handling of vitamin A aldehyde in outer segments of photoreceptor cells with the result that phototoxic bisretinoids of lipofuscin, including A2E, form in abundance. Disc shedding and subsequent phagocytosis of the outer segments by RPE cells leads to significant lysosomal accumulations of lipofuscin. This mechanism has been largely connected to STGD1-associated features such as increased fundus autofluorescence,[4] yellow pisciform flecks, and progressive atrophy of the outer retinal layers, among other findings. As such, RPE cells and photoreceptors have been implicated to be the primary cellular effectors in the onset and progression of STGD1. A diagnosis of STGD1, and the subsequent decision to screen *ABCA4*, has been largely reliant on the identification of such retinal features resulting from RPE and/or photoreceptor changes; however, Burke et al.[5] reported a single case of a young patient with STGD1 exhibiting an unusual thickening of the external limiting membrane (ELM) band on spectral-domain optical coherence tomography (SD-OCT) in the absence of other functional and structural changes to the retina. The ELM,

sometimes referred to as the outer limiting membrane, consists of both homotypic (Müller cell-to-Müller cell) and heterotypic (Müller cell-to-photoreceptor) adherens junctions[6,7] (Fig. 1), providing structural support for proper cellular organization, integrity, and alignment in the retinal anatomy.[8–11] Disruption of the ELM has been shown to trigger a variety of responses ranging from cellular migration from the subretinal space into the outer nuclear layer (ONL) and, conversely, movement of glial-derived progenitor cells into the outer retina.[12,13]

Under the suspicion that ELM abnormalities occur in early stages of STGD1, we examined a cohort of 26 clinically diagnosed and genetically confirmed patients soon after disease onset. Symptomatic changes indicative of early-onset STGD1 typically begin within the first and second decades of life.[14] Therefore, the inclusion criteria were limited to those patients first examined when aged younger than 20 years.

MATERIALS AND METHODS

Patients and Clinical Evaluation

A retrospective review of 437 patients with a clinical diagnosis and genetic confirmation of STGD1 was conducted at the department of ophthalmology, Columbia University. Within this cohort, SD-OCT and fundus autofluorescence (AF; 488 nm)

images were available for 179 patients. From this group, patients who presented to the clinic for SD-OCT and autofluorescence imaging before age 20 years were included in the study. The estimated disease duration for each patient was defined to be the age at first examination minus reported age of symptomatic onset. All patients were consented before participating in the study under the institutional review board protocol #AAAI9906 approved by the Institutional Review Board at Columbia University. The study adhered to tenets set out in the Declaration of Helsinki. Each patient underwent a complete ophthalmic examination reviewed by a retinal physician (SHT, SB), including slit-lamp and dilated fundus examinations. The generalized function of the retina was assessed with ERG data available for 19 patients within the cohort. Vision was assessed by the measurement of best corrected visual acuity (BCVA; Snellen), while further structural assessments were made using color fundus photography, autofluorescence, and SD-OCT.

Data Acquisition

Spectral-domain optical coherence tomography scans and corresponding fundus images were acquired using an OCT device (Spectralis HRA+OCT; Heidelberg Engineering, Heidelberg, Germany). Fundus AF and near-infrared reflectance images were obtained using a confocal scanning-laser ophthalmoscope (cSLO, Heidelberg Retina Angiograph 2; Heidelberg Engineering). Fundus AF images were acquired by illuminating the fundus with an argon laser source (488 nm) and viewing the resultant fluorescence through a band-pass filter with a short wavelength cutoff at 495 nm. Color fundus photos were obtained with an infrared fundus camera (FF 450 plus Fundus; Carl Zeiss Meditec AG, Jena, Germany).

Electroretinograms in each patient were recorded using a commercial electrophysiology system (Diagnosys Espion Electrophysiology System; Diagnosys LLC, Littleton, MA, USA). For each recording, the pupils were maximally dilated and measured before full-field ERG (FFERG) testing using guttate tropicamide (1%) and phenylephrine hydrochloride (2.5%). The corneas were anesthetized with guttate proparacaine 0.5%. Silver impregnated fiber electrodes (DTL; Diagnosys LLC) were used with a ground electrode on the forehead. Full-field ERGs to test generalized retinal function were performed using extended testing protocols incorporating the International Society for Clinical Electrophysiology of Vision standard.[15]

Image Analyses

Quantitative analyses of the ELM and inner segment ellipsoid (ISe) band, also referred to as the ellipsoid zone band, were conducted on high-resolution SD-OCT scans (1536 pixels in length; Heidelberg Engineering) of the right eye in 24 STGD1 patients (mean age, 12.9 years; range, 5–19 years) and 30 age-matched controls (age range, 4–20 years; mean age, 12.5 years). The sampling area for each measurement was assigned to a position half the distance between the foveal center and the nasal edge of the optic disc, a location measured with the ruler tool within the ophthalmic software (Heidelberg Explorer Software; Heidelberg Engineering). Analysis of the designated area in the macula was not possible in two patients (P10, P23) due to progressed atrophy. Thickness and reflectivity values were averages between measurements made manually by two independent observers (WL, KN; measurements available in Supplementary Table S1) on the ophthalmic software (Heidelberg Engineering). Reflectivity of the ELM and ISe bands on SD-OCT was assessed by obtaining the maximum pixel gray values (peaks) corresponding to the ELM and ISe of a vertically positioned pixel intensity profile (reflectivity profile), perpen-
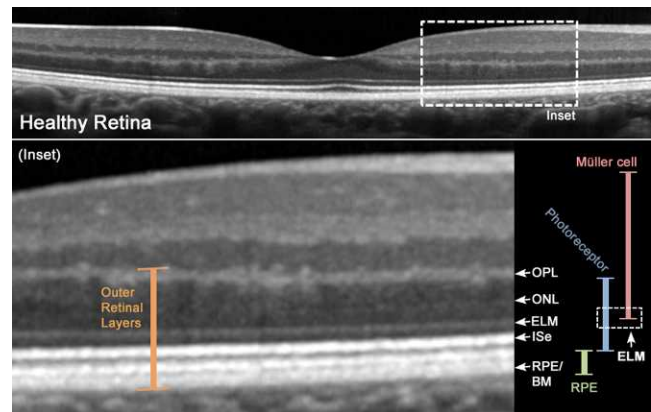
FIGURE 1. Spectral-domain optical coherence tomography scan of the macular region of the retina in the right eye of a healthy subject. *Inset*: The *orange bracket* (*left*) marks the layers within the outer retina that include the outer plexiform layer, ONL, ELM, ellipsoid zone or ISe, and RPE/Bruch membrane complex (RPE/BM). The ELM is the physical intersection, through adherens junctions, between photoreceptors and Müller cell processes.

dicular to the RPE layer. Pixel intensity profiles were generated and analyzed with ImageJ software (http://imagej.nih.gov/ij/; provided in the public domain by the National Institutes of Health, Bethesda, MD, USA). Intraclass correlation coefficients (ICC) were calculated to assess interobserver agreement and statistical comparisons were made by unpaired Student t-tests (two-tailed) and deemed statistically significant if $P < 0.05$ in statistical software used (SPSS Statistics 16.0 for Windows; SPSS, Inc., Chicago, IL, USA).

Genetic Analyses

Screening of the *ABCA4* gene was performed in all patients by two methods. First, screening with the *ABCA4* microarray was performed on all study subjects followed by direct Sanger sequencing to confirm identified changes, as previously described.[16] The DNA of those patients in whom only one or no *ABCA4* mutations were identified with the array was screened by next-generation sequencing as described before[17] or with a different method where all 50 exons and exon-intron boundaries of the ABCA4 gene were amplified using a commercial amplicon-based protocol (Illumina TruSeq Custom Amplicon; Illumina, Inc., San Diego, CA, USA), followed by sequencing on a commercial platform (Illumina MiSeq; Illumina, Inc.). The next-generation sequencing reads were analyzed and compared with the reference genome GRCh37/hg19, using variant discovery software (NextGENe; SoftGenetics LLC, State College, PA, USA). All detected possibly disease-associated variants were confirmed by Sanger sequencing and analyzed with mutation diagnostic software (Alamut, provided in the public domain by http://www.interactive-biosoftware.com; Interactive Biosoftware, Rouen, France). Segregation of the identified *ABCA4* variants with the disease was analyzed in all but one patient.

RESULTS

### Clinical and Genetic Evaluation

A retrospective analysis of 26 clinically diagnosed STGD1 patients with the disease onset in the first two decades of life at the initial examination (mean age, 12.9 years; range, 5–19 years) was performed and the demographic, clinical, and
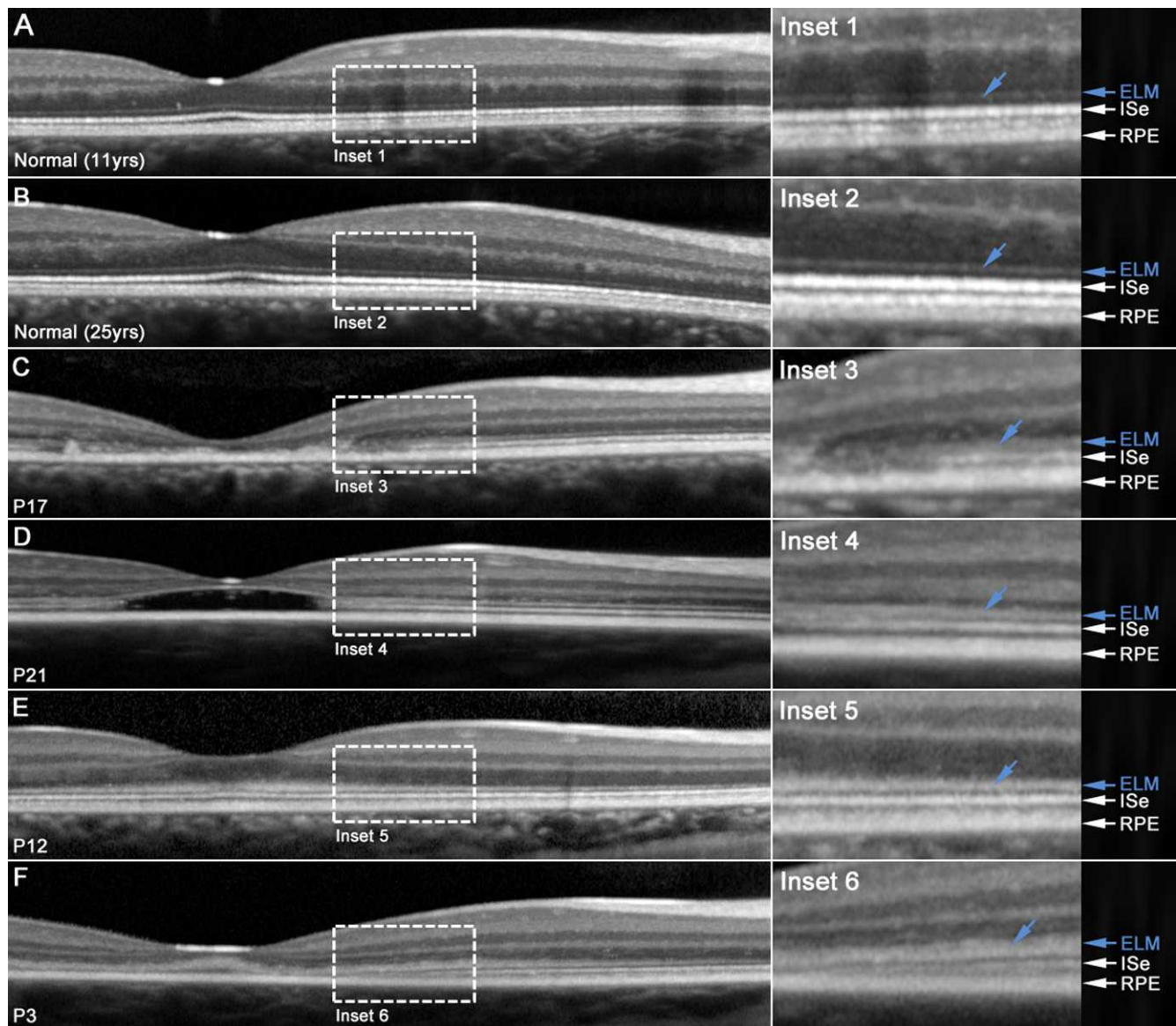
FIGURE 2. The spectrum of increased thickening and reflectivity of the ELM seen on SD-OCT in normal and STGD1 patients. (**A, B**) Retinas of two unaffected individuals within the age range of the patient cohort exhibited a thin and faint ELM (*blue arrows*) in comparison with the underlying ISe band and RPE below (*insets 1, 2*). The ELM appeared to be evidently thickened and more discernible (hyperreflective) in STGD1 patients: (**C**) *inset 3*, (**D**) *inset 4*, (**E**) *inset 5*, and (**F**) *inset 6*, (*blue arrows*).

genetic results are summarized in Table 1. Disease duration ranged between 0.5 to 8 years. Seven patients (P3, P4, P6, P7, P10, P12, P24) were asymptomatic at initial presentation and were discovered through an affected sibling. At least two (expected) disease-causing *ABCA4* variants were identified in all patients except one sibling pair (P2, P3) and one patient of African American descent (P20) in whom only one disease-associated allele has been found thus far. Segregation analyses confirmed the phase (different parental origin) of the disease-associated *ABCA4* alleles in all but one patient. A full fundus examination was largely unremarkable for other ocular findings not typically associated with STGD1 disease. At the time of examination, all patients were found to be phenotypically categorized in either stage 1 (54%) or 2 (46%) of the clinical disease spectrum of STGD1 as defined by Fishman et al.[18] One patient (P12) presented asymptomatically with no apparent changes on funduscopy while eight others (31%) presented with the bull's eye maculopathy phenotype. Upon further examination, 18 (69%) patients either initially presented with, or eventually developed, yellow pisciform flecks. Autofluorescence (AF) imaging revealed the presence of "fine macular dots" in 14 patients (54%), which were analogous to those previously described in young STGD1 patients.[19] The degree of flecking in these patients was determined based on spatial distribution and confluence. Patients were categorized as "early" if flecks were small and centrally localized around the fovea, "mid" if flecks were relatively larger and populated throughout the macula, and "late" if flecks appeared beyond the vascular arcades and exhibited darkening and resorption. Best-corrected visual acuities were highly variable, ranging from 20/20 to 20/400 in both eyes. All patients exhibited varying degrees of electrophysiological function and were categorized into phenotypic subtypes according to Lois et al.[20] Full-field electroretinogram (ERG) results were available for 19 patients, of which 13 (68%) exhibited normal generalized scotopic and photopic function (group 1) and six (32%) had
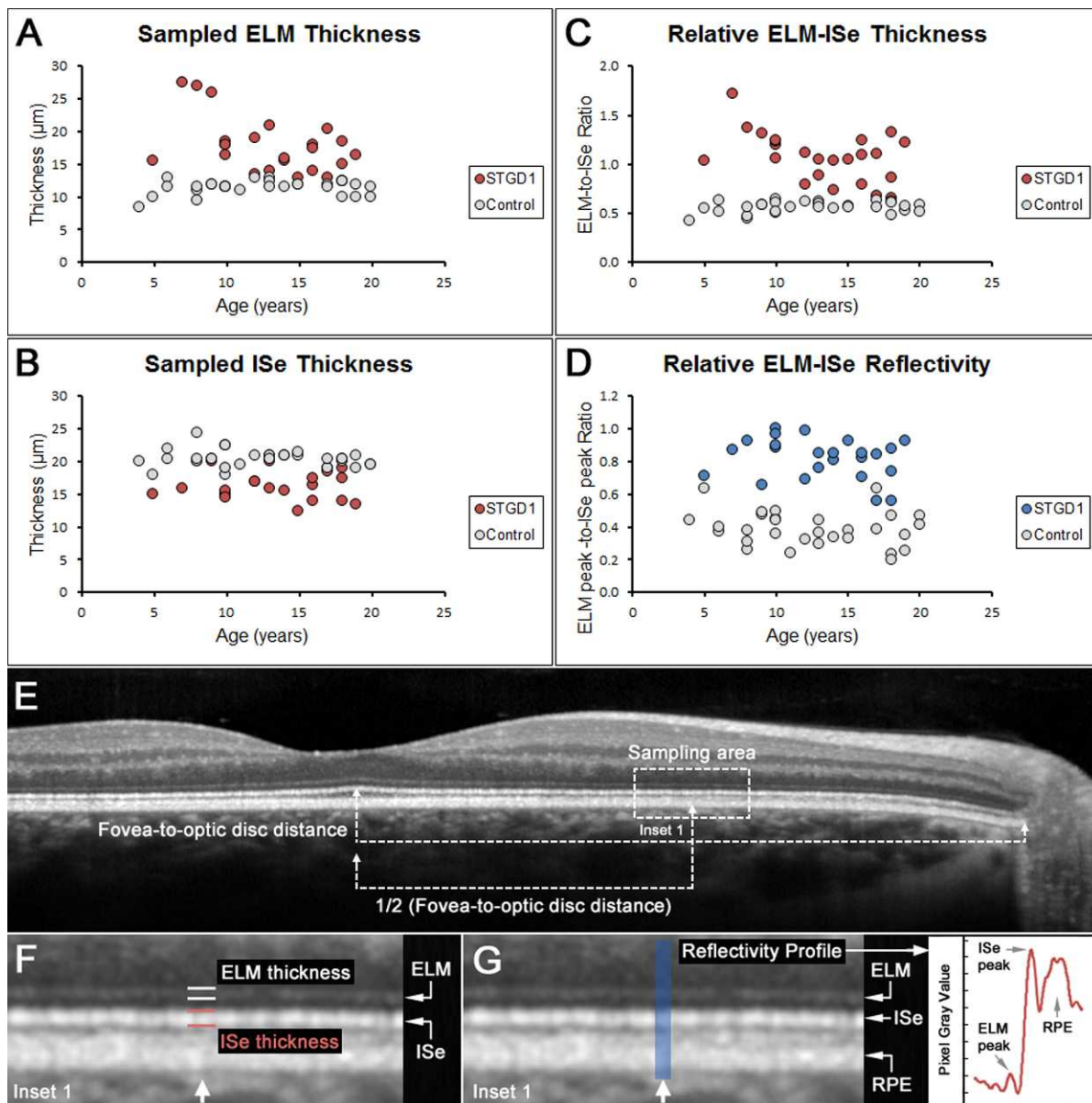
FIGURE 3. Quantitative analyses of ELM and ISe band thickness and reflectivity on SD-OCT. Thickness (µm) of the ELM and ISe were measured at a consistent position within the macula in 24 STGD1 patients (*red circles*) and 30 age-matched controls (*gray circles*). Analysis of the designated area of the macula was not possible in two patients (P10, P23) due to progressed atrophy. (**A**) Thickness of ELM in the measured areas was significantly greater ($P < 0.0001$) in STGD1 patients compared with unaffected individuals, (**B**) whereas the thickness of the ISe at the same location was thinner in STGD1 ($P < 0.0001$). (**C**) The relative ELM/ISe thickness (calculated as the ratio between ELM and ISe) within normal subjects consistently fell within 0.5 (ISe band is approximately two times thicker than ELM band); an overall larger and more variable relative ELM/ISe thickness ($P < 0.0001$) was observed in STGD1 patients. (**D**) Relative reflectivities of the ELM-to-ISe bands where significantly more intense ($P < 0.0001$) in STGD1 patients compared with normal controls. (**E**) The sampling area for each measurement was assigned to half the distance between the foveal center and the nasal edge of the optic disc. (**F**) Thickness measurements where made manually by two independent observers. (**G**) Comparative band reflectivity values were obtained from the maximum pixel gray values (peaks) corresponding to the ELM and ISe of a vertically positioned pixel intensity profile (reflectivity profile).

amplitudinal reductions and implicit time delays in the photopic system (group 2).

Enhanced ELM Thickening and Discernibility

Qualitative (Fig. 2) and quantitative analyses of the ELM and ISe bands on SD-OCT revealed consistent and significant differences between STGD1 patients and age-matched controls. The thickness of the ELM band in the measured area (Fig. 3F) was significantly greater (mean = 17.69 µm, SD = 4.23) in STGD1 patients, particularly in the three younger patients (P3, P10, P16) compared with unaffected individuals (mean = 11.45 µm, SD = 1.08, $P < 0.0001$; Fig. 3A). A mild downward trend in ELM thickness with age was noted ($r^2 = 0.21$), while ELM thickness appeared to be relatively constant in the control group. In this same area, STGD1 patients exhibited a thinner (mean = 16.65 µm, SD = 2.34, $P < 0.0001$) ISe band compared with unaffected individuals (mean = 20.64 µm, SD = 1.34, $P <$

Investigative Ophthalmology & Visual Science

TABLE 1. Summary of Demographic, Clinical and Genetic Characteristics

Patient	Age, y	Ethnicity	BCVA Snellen, logMAR OD	BCVA Snellen, logMAR OS	Fishman Stage	FFERG Group	Flecks	Estimated Disease Duration, y†	ABCA4 Disease-Associated Alleles Allele 1	ABCA4 Disease-Associated Alleles Allele 2
P1	10	Caucasian	20/30 (0.18)	20/25 (0.01)	1	1	Early	1	p.E160*	p.R1108C
P2	10	Caucasian	20/70 (0.54)	20/80 (0.60)	2	2	Early-late	0.5	p.[L541P;A1038V]	ND
P3	7	Caucasian	20/40 (0.30)	20/30 (0.18)	1	1		ND	p.[L541P;A1038V]	ND
P4	13	Caucasian	20/80 (0.60)	20/50 (0.40)	2	1	Mid	ND	p.P1380L	c.5714+5G>A
P5	14	Caucasian	20/200 (1.00)	20/150 (0.88)	1	1	Late	0.5	p.P1380L	c.5714+5G>A
P6	13	Caucasian	20/40 (0.30)	20/50 (0.40)	2	1	Late	ND	p.[L541P;A1038V]	p.L2027F
P7	8	Caucasian	n/a	n/a	1	n/a		ND	p.[L541P;A1038V]	p.L2027F
P8	10	Caucasian	20/40 (0.30)	20/80 (0.60)	1	1	None-early	1	p.R1108C	p.Q1412*
P9	14	Caucasian	20/100 (0.70)	20/100 (0.70)	2	1	Early-late	0.5	p.T972N	p.L2027F
P10	9	Caucasian	20/150 (0.88)	20/400 (1.30)	2	1	Late	ND	c.5312+1G>A	p.R2030*
P11	15	Caucasian	20/200 (1.00)	20/200 (1.00)	2	2	Mid-late	3	p.L2027F	p.R2077W
P12	5	Caucasian	20/30 (0.18)	20/40 (0.30)	1	n/a		ND	c.5018+2T>C	p.G1961E
P13	10	Caucasian	20/200 (1.00)	20/200 (1.00)	2	2	Mid	4	p.[L541P;A1038V]	p.R1640W
P14	12	Caucasian	20/200 (1.00)	20/200 (1.00)	2	2	Late	6	p.[L541P;A1038V]	p.R1640W
P15	16	Caucasian	20/200 (1.00)	20/200 (1.00)	2	n/a	Mid-late	8	p.K346T	p.T1117I
P16	9	Caucasian	20/150 (0.88)	20/150 (0.88)	1	n/a		1	p.P1380L	p.G1961E
P17	18	Caucasian	20/40 (0.30)	20/150 (0.88)	1	1	Early	3	p.P1380L	p.G1961E
P18‡	18	Caucasian	20/150 (0.88)	20/150 (0.88)	2	1	Late	4	p.[L541P;A1038V]	p.L2027F
P19	16	Caucasian	20/150 (0.88)	20/150 (0.88)	1	n/a	Early	6	p.G863A	p.[W1408R;R1640W]
P20	18	African American	20/125 (0.80)	20/50 (0.40)	2	2	Mid	5	p.R1640W	ND
P21	12	Caucasian	20/50 (0.40)	20/50 (0.40)	1	1		6	p.W821R	p.C2150Y
P22	17	Indian	20/40 (0.30)	20/100 (0.70)	1	n/a	Mid	3	p.G1961E	c.6729+4_+18del
P23	10	Indian	20/400 (1.30)	20/400 (1.30)	2	2	Early	3	c.885delC	p.R537C
P24	19	Caucasian	20/20 (0.00)	20/20 (0.00)	1	n/a		ND	p.G863A	c.5898+1G>A
P25	16	Middle Eastern	20/80 (0.60)	20/100 (0.70)	1	1		4	p.A1773V	p.G1961E
P26	17	Caucasian	20/150 (0.88)	20/200 (1.00)	1	1		2	p.K1547*	p.R2030Q

ND, not determined; n/a, not available.

† Estimated disease duration is defined as age of first examination minus reported age of onset.

‡ Segregation analysis was not performed.

TABLE 2. Quantitative Thickness and Reflectivity Sampling in SD-OCT Scans

| | SD-OCT Thickness, µm | | | | SD-OCT Reflectivity, Gray Value | | | |
| | ISe | | ELM | | ISe | | ELM | |
Mean Measurements	STGD1	Control	STGD1	Control	STGD1	Control	STGD1	Control
Mean	16.65	20.64	17.69	11.45	170.40	210.58	139.5	81.15
Standard deviation	2.34	1.34	4.23	1.08	19.24	31.32	24.40	22.76
Standard error	0.48	0.24	0.86	0.20	3.93	5.72	4.98	4.16
Unpaired *t*-test			SD-OCT thickness, µm				SD-OCT reflectivity	
	ELM: STGD1 vs. control		ISe: STGD1 vs. control		ELM-ISe ratio: STGD1 vs. control		ELM-ISe ratio: STGD1 vs. control	
P value	<0.0001		<0.0001		<0.0001		<0.0001	

0.0001; Fig. 3B). To assess the thickness of the ELM relative to the ISe, the calculated ratios of ELM/ISe in the patients were compared with the control ratios (Fig. 3C). Ratios of ELM/ISe in unaffected individuals fell consistently within the 0.5 range, indicating a 1-to-2 relationship between the thickness of ELM and ISe bands on SD-OCT. Thickness ratios of ELM/ISe in STGD1 patients, while more variable, were significantly greater ($P < 0.0001$) than the control group (Fig. 3C). Band reflectance on SD-OCT was assessed by comparing the brightest pixel (vertical gray value profile peak) of the ELM and ISe bands (Fig. 3G). To compare patients while accounting for scan normalization, reflectance values were compared as ratios for each patient. The reflectance ratios in STGD1 patients were significantly greater ($P < 0.0001$) than those of the control group (Fig. 3D). Quantitation in two patients, P10 and P23, was impossible due to progressed atrophy in the measurement area; however, ELM thickening and increased reflectivity was qualitatively observed in their respective SD-OCT scans in less-affected areas of the macula. Statistical results are summarized in Table 2. Calculated ICCs revealed acceptable agreement between both observers for each measurement (Table 3).

Foveal ELM Protuberance and ONL Deposition

A subgroup of four patients—P1, P3, P4 (Fig. 4), and P24 (not shown)—exhibited an unusual foveal lesion characterized by an isolated concave protuberance or bulging of the ELM that was thickened and hyperreflective and that encased a small area of ISe despite surrounding regions of atrophic changes. The ELM protuberance correlated with areas of hypoautofluorescence in the AF image (dotted position markers). Patients P1, P3 (Fig. 4), and P24 (not shown) exhibited fine macular dots on AF within areas of relatively preserved ISe and RPE layers in the central macula, whereas P4 exhibited more progressive changes, including central mottling and macular flecks.

In addition to ELM thickening, SD-OCT revealed small, hyperreflective deposits within the ONL of all patients (Fig. 5, red arrows, and insets 1, 4, and 6). This feature was not as apparent in more distal areas of the central lesion (Fig. 5, insets 2, 3, and 5). Such findings were correlated with areas marked with hyperautofluorescent mottling and flecking.

Longitudinal Changes

Progression data following two or more time points, 1 year apart, revealed variable changes in each patient. Out of 17 patients who initially presented with yellow pisciform flecks, two (P2, P9) progressed from "early" to "late" stage patterns; two others (P11, P15) presented at "mid" stage and developed a "late" pattern; and one (P8) appeared unaffected and developed an "early" pattern. Serial SD-OCT imaging revealed a receding ISe and apparent RPE thinning over time at the leading edge of the central lesion of atrophy. No apparent changes to the ELM were observed in this time period; however, a consistent discordance between the position of ISe loss (Fig. 6, red arrows) and ELM loss (Fig. 6, white arrows) was noted. In almost all observed cases, the ISe band appeared to recede earlier than the ELM on SD-OCT (Fig. 6, red and white arrows).

DISCUSSION

Examination of 26 genetically confirmed, early-onset (disease onset was strictly confined to age < 20 years) STGD1 patients in this study produced several findings, of which the most prominent were apparent changes to the ELM on SD-OCT. In all examined patients, an observable thickening of the ELM and increased discernibility was evident in the macula, particularly in areas of relatively intact photoreceptors and RPE. In other areas, this observation was also concurrent with other STGD1-associated findings such as early pisciform flecks, local hyperautofluorescence and centrally confined areas of hypoautofluorescence. One case, P12, however, exhibited the abnormal ELM without any other apparent pathology on fundoscopy and was asymptomatic (Fig. 2E). In all except two patients in whom quantitation was not possible, thickness measurements confirmed the clinically observed prominence of the ELM and was observed to gradually decrease (downward sloping trend line, $r^2 = 0.21$) with increasing patient age. This trend toward thinning was largely obviated by three younger patients (P3, P10, P16) who each exhibited a significantly thickened ELM at the measured position. If confirmed in a larger group of patients, this trend may suggest that the mechanism behind the observed ELM thickening may be a

TABLE 3. Intraclass Correlation Coefficients of SD-OCT Measurements

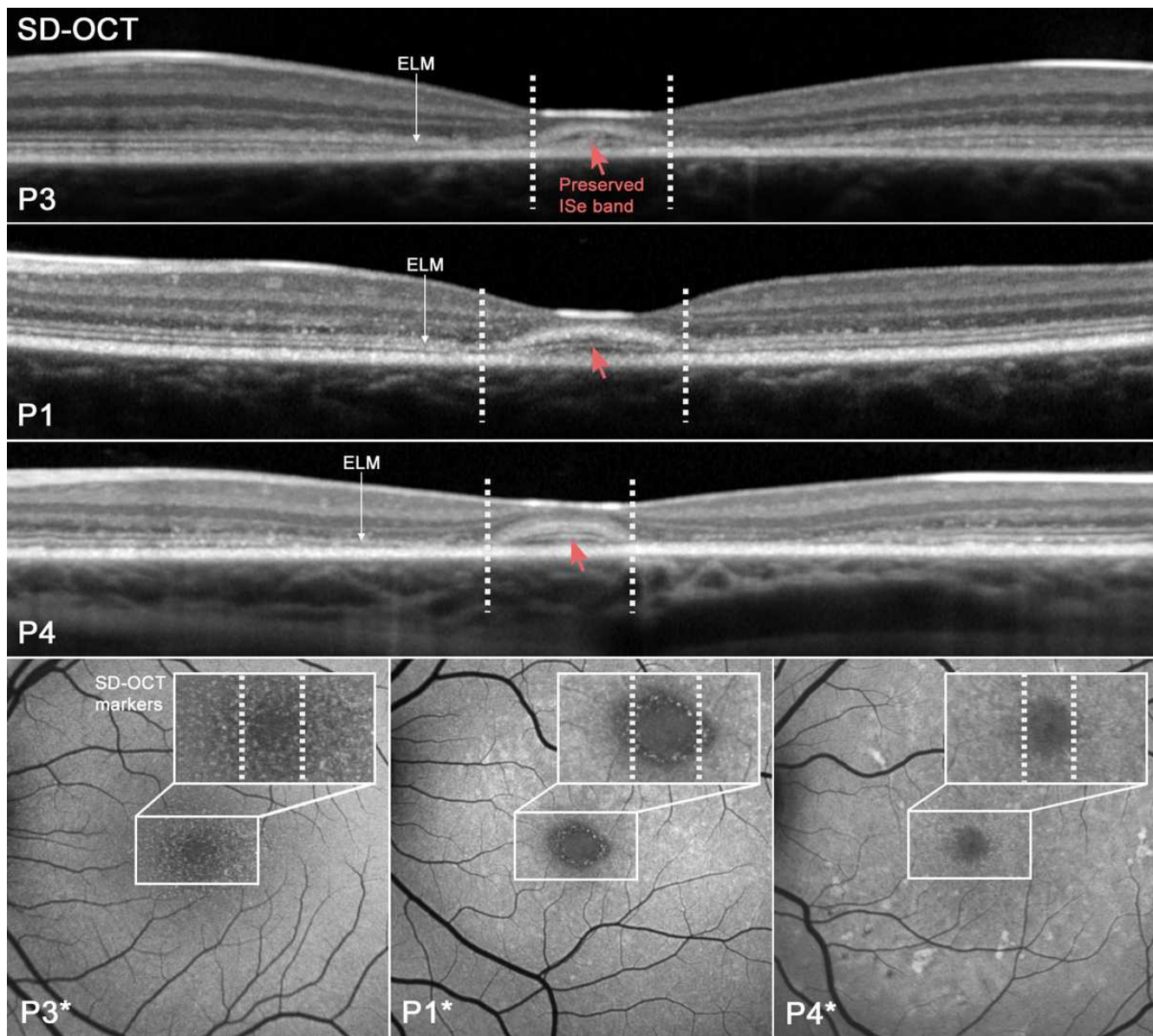|	STGD1 Patients	Unaffected Individuals
Sampled ELM thickness, µm	0.948 (0.782–0.982)	0.836 (0.659–0.922)
Sampled ELM reflectivity, gray value	0.938 (0.861–0.973)	0.920 (0.830–0.962)
Sampled ISe thickness, µm	0.796 (0.472–0.915)	0.874 (0.738–0.940)
Sampled ISe reflectivity, gray value	0.799 (0.535–0.913)	0.876 (0.736–0.941)

The 95% confidence intervals are in parentheses.

FIGURE 4. Foveal protuberance or bulging of an area of hyperthickened and reflective ELM in STGD1 patients on SD-OCT. The ELM in P3 appeared to be continuous throughout the macula despite the bulge while a more intensely reflective and thick bulge in P1 was partially intermittent at the base of the ELM bulge. The ELM was observably absent along areas adjacent to the bulge in P4. A small area of the ellipsoid zone was preserved within the ELM bulges in all patients exhibiting this feature (*red arrows*). *Dotted vertical lines* on the spectral-domain optical coherence tomography scans demarcate the corresponding areas on AF imaging (P3*, P1*, P4*). The base edge of each bulge corresponded with areas of hypo-AF surrounded by fine reflective macular dots.

transient event in STGD1. The ISe band (at the same measurement location) appeared to be significantly thinner compared with unaffected individuals—a finding which could suggest structural photoreceptor abnormalities at the early stage of the disease. The finding of increased reflectivity also substantiated the heightened visibility of the ELM in STGD1 patients. The inherent source of band reflectivity on SD-OCT is largely unknown. It has been suggested that mitochondria may partly contribute to OCT visibility, among other structures.[21] Decreased ISe band intensities, as well as thinning, has been described in patients with diminished cone function though no additional information pertaining to its cellular origins were made.[22] Certain limitations to this quantitation method, including spatially restricted area of measurements, image quality, intersubject scan normalization, among others, are

likely to introduce errors, further necessitating more extensive analyses in addition to those that have been previously described.[23,24] However, a comparative study has confirmed the reproducibility of SD-OCT data from the instrument (Heidelberg Engineering) used in this study.[25] Additional observations included the finding of a hyperthickened ELM forming a round concave bulge (protuberance) over the fovea covering an area of preserved photoreceptors in four cases (Fig. 4). In addition to changes to the ELM itself, all patients also exhibited granular depositions within the ONL in areas near the central atrophic lesion in the macula (Fig. 5).

Given the limitation of SD-OCT in providing information regarding precise cellular processes, further studies are warranted to confirm our conclusions; however, several hypotheses can be generated from these findings. First,

FIGURE 5. Accumulation of reflective deposits within the outer nuclear layer in STGD1 patients. Three representative patients (P9, P19, P16) exhibiting various phenotypic features of STGD1 seen on AF imaging presented with thickened external limiting membrane bands on SD-OCT along with an accumulation of reflective deposits in areas near the central lesion, flecks and/or hyper-AF (*inset, inner*) while less affected distal areas (*inset, outer*) did not exhibit this feature or to a lesser extent.

changes in the ELM can be attributed to the (mis)interaction between photoreceptors and Müller cell processes or homotypically between Müller cells. Müller cells become reactive to many pathologic stimuli in the retina—whether extrinsic or intrinsic. This process, known as gliosis, involves hypertrophy, proliferation, migration of glial cells or their processes, and glial scarring at the site of insult.[26] Although literature on histopathology of STGD1 is limited, one study observed reactive Müller cell hypertrophy in the dissected retina of an STGD1 patient.[27] Gliosis can be provoked by local photocoagulation laser injury[13] or intravitreal injections,[28] which perturb cellular layers, particularly photoreceptors. The common response to each of these stimuli has been shown to be a rapidly reactive response of Müller cells at the site of injury and in other cases throughout the entire retina.[29] Likewise, other apoptotic retinal degenerative diseases, such as retinitis pigmentosa (RP), have triggered early Müller cell responses to cellular stress wherein the hypertrophic proliferation of Müller cells was shown to precede any significant involvement of other retinal cell layers.[30] Müller cell hypertrophy and, interestingly, the formation of a dense fibrotic layer outside of the inner nuclear layer has been observed in the early stages of disease phenotype in *Aipl*$^{-/-}$ mice, a model of Leber congenital amaurosis (LCA), RP, and cone-rod dystrophy.[29] Although RP and LCA are etiologically distinct from

STGD1, each condition may share a common cellular response to stress. Such differing etiologies may also result in varying manifestations at the clinical level; for instance, many factors specific to each condition including rate of cell loss, intercellular interactions, or local changes in the chemical milieu may affect Müller cell responses or visibility of this process on SD-OCT.

The initial consequence of gliosis in the retina has been described as early cellular attempts by Müller cells to protect photoreceptors from further damage by the secretion of neuroprotective substances and antioxidants by facilitated phagocytosis of toxic compounds; however, a prolonged, persistent response may have oppositely damaging effects.[31-33] Under the same context of cellular preservation, the formation of outer retinal tubulation which has been histologically shown to consist of preserved photoreceptors, represents the protective capacity of Müller cells, though these processes have been found to occur in later stages of retinal dystrophies (Freund KBSK, et al. *IOVS* 2014;55:ARVO E-Abstract 4014 and Refs. 34 and 35). Furthermore, the mechanism and proliferative potential of Müller cells in neural regeneration has also been extensively examined.[12,36,37] These studies observed glial-derived progenitor cells migrating through the ONL toward the stimulating stress. By extension, our observation of hyperreflective deposits in the ONL observed in areas near
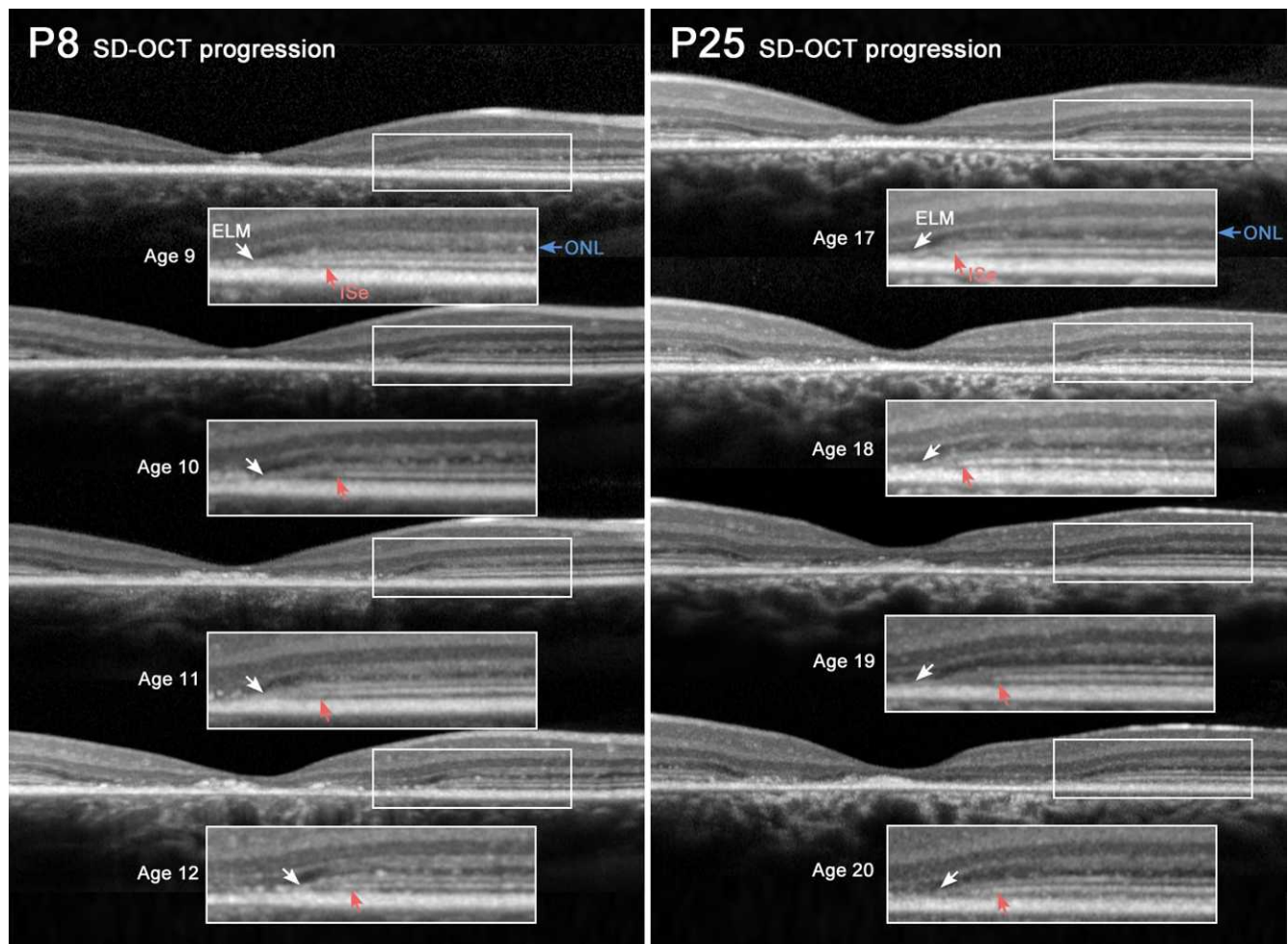
FIGURE 6. Longitudinally documented SD-OCT scans taken 1 year apart in STGD1 patients. No apparent structural changes to the ELM, with respect to thickening, were noted; however, the receding edge of the ELM (*white arrows*) visibly degenerated more slowly than that of the ISe band (*red arrows*) over time.

the active lesion in each patient (Fig. 5) may be a recapitulation of this process such that the observed thickening of the ELM, as an anatomical barrier, is a subsequent accumulation of glial cells migrating toward outer retinal stress in the setting of STGD1.

The foveal protuberance or bulging of hyperthickened and reflective ELM in the three of four cases (P1, P3, P4, Fig. 4) presented here, was not fully understood though the preserved area of ISe within this encapsulation resembles the foveal sparing phenomenon, an infrequent subphenotype in STGD1. A recent study examined distinct clinical and genetic features of foveal sparing in a cohort of STGD1 patients though its precise genetic and clinical etiology remains unclear.[38,39] The occurrence of this phenotype in the fovea may reflect the high density of cones in this region.[40] Recent attention has been directed toward the discovery of an alternative mechanism of photopigment regeneration in cones.[41] Following exposure to bright light, cones regenerate visual pigment nearly 10 times faster than rods.[42] Pigment regeneration in photoreceptors is known to be rate-limited by the availability of recycled chromophores, which are regularly supplied by RPE cells, though at nowhere near the rate required to support the rapid dark-adaption of cones.[43,44] Given this incompatible supply-and-demand dynamic, evidence was found for an alternate, RPE-independent, source of cone-specific chromophores (11-*cis* ROL) by Müller cells.[45–47] Even more interestingly, the ratio

of Müller cells to cones in primate fovea has been found to be 1:1, further supporting a more functionally intimate relationship between the two cell types.[48,49] It may thus be reasonable to hypothesize that the observed protuberant ELM response (Fig. 4) may be a visible indicator of an attempt to compensate for the presence of underlying lipofuscin-laden defective RPE cells, by buttressing interactions between Müller cells and cones thereby facilitating cone access to 11-*cis* retinol from Müller cells. Adaptations such as this could extend the lifespan of cones in this region and give rise to the foveal sparing phenomenon in STGD1.

Summarizing the current and previous findings, we suggest that the observed thickening of the ELM in STGD1 patients may be an early protective response of Müller cells to the stress elicited by ABCA4-deficiency. Furthermore, the severe protuberant response within the foveal region, in conjunction with the utilization of the Müller cell-assisted cone visual cycle, may contribute to a transient survival of cones resulting in the foveal sparing phenomenon exhibited by some affected patients. These conclusions may also extend to late-onset, or all STGD1 patients; however, the precise onset age in these cases is often difficult to define and such features observed in early-onset cases may have dissipated by the time these patients are examined. Continued studies of these processes may be fruitful for providing novel therapeutic insights for

STGD1, especially given the regenerative potential of glial cells in the retina.

References

1. Burke TR, Tsang SH. Allelic and phenotypic heterogeneity in ABCA4 mutations. _Ophthalmic Genet_. 2011;32:165–174.

2. Michaelides M, Hunt DM, Moore AT. The genetics of inherited macular dystrophies. _J Med Genet_. 2003;40:641–650.

3. Allikmets R, Singh N, Sun H, et al. A photoreceptor cell-specific ATP-binding transporter gene (ABCR) is mutated in recessive Stargardt macular dystrophy. _Nat Genet_. 1997;15: 236–246.

4. Burke TR, Duncker T, Woods RL, et al. Quantitative fundus autofluorescence in recessive Stargardt disease. _Invest Ophthalmol Vis Sci_. 2014;55:2841–2852.

5. Burke TR, Yzer S, Zernant J, Smith RT, Tsang SH, Allikmets R. Abnormality in the external limiting membrane in early Stargardt disease. _Ophthalmic Genet_. 2013;34:75–77.

6. Paffenholz R, Kuhn C, Grund C, Stehr S, Franke WW. The arm-repeat protein NPRAP (neurojungin) is a constituent of the plaques of the outer limiting zone in the retina, defining a novel type of adhering junction. _Exp Cell Res_. 1999;250:452–464.

7. Williams DS, Arikawa K, Paallysaho T. Cytoskeletal components of the adherens junctions between the photoreceptors and the supportive Müller cells. _J Comp Neurol_. 1990;295: 155–164.

8. Chen X, Zhang L, Sohn EH, et al. Quantification of external limiting membrane disruption caused by diabetic macular edema from SD-OCT. _Invest Ophthalmol Vis Sci_. 2012;53: 8042–8048.

9. Omri S, Omri B, Savoldelli M, et al. The outer limiting membrane (OLM) revisited: clinical implications. _Clin Ophthalmol_. 2010;4:183–195.

10. Rich KA, Figueroa SL, Zhan Y, Blanks JC. Effects of Müller cell disruption on mouse photoreceptor cell development. _Exp Eye Res_. 1995;61:235–248.

11. Wakabayashi T, Oshima Y, Fujimoto H, et al. Foveal microstructure and visual acuity after retinal detachment repair: imaging analysis by Fourier-domain optical coherence tomography. _Ophthalmology_. 2009;116:519–528.

12. Ooto S, Akagi T, Kageyama R, et al. Potential for neural regeneration after neurotoxic injury in the adult mammalian retina. _Proc Natl Acad Sci U S A_. 2004;101:13654–13659.

13. Tackenberg MA, Tucker BA, Swift JS, et al. Müller cell activation, proliferation and migration following laser injury. _Mol Vis_. 2009;15:1886–1896.

14. Weleber RG. Stargardt's macular dystrophy. _Arch Ophthalmol_. 1994;112:752–754.

15. Marmor MF, Fulton AB, Holder GE, et al. ISCEV Standard for full-field clinical electroretinography (2008 update). _Doc Ophthalmol_. 2009;118:69–77.

16. Jaakson K, Zernant J, Kulm M, et al. Genotyping microarray (gene chip) for the ABCR (ABCA4) gene. _Hum Mutat_. 2003; 22:395–403.

17. Zernant J, Schubert C, Im KM, et al. Analysis of the ABCA4 gene by next-generation sequencing. _Invest Ophthalmol Vis Sci_. 2011;52:8479–8487.

18. Fishman GA, Stone EM, Grover S, Derlacki DJ, Haines HL, Hockey RR. Variation of clinical expression in patients with Stargardt dystrophy and sequence variations in the ABCR gene. _Arch Ophthalmol_. 1999;117:504–510.

19. Fujinami K, Singh R, Carroll J, et al. Fine central macular dots associated with childhood-onset Stargardt Disease. _Acta Ophthalmol_. 2014;92:e157–e159.

20. Lois N, Holder GE, Bunce C, Fitzke FW, Bird AC. Phenotypic subtypes of Stargardt macular dystrophy-fundus flavimaculatus. _Arch Ophthalmol_. 2001;119:359–369.

21. Spaide RF, Curcio CA. Anatomical correlates to the bands seen in the outer retina by optical coherence tomography: literature review and model. _Retina_. 2011;31:1609–1619.

22. Hood DC, Zhang X, Ramachandran R, et al. The inner segment/outer segment border seen on optical coherence tomography is less intense in patients with diminished cone function. _Invest Ophthalmol Vis Sci_. 2011;52:9703–9709.

23. Hood DC, Cho J, Raza AS, Dale EA, Wang M. Reliability of a computer-aided manual procedure for segmenting optical coherence tomography scans. _Optom Vis Sci_. 2011;88:113–123.

24. Hood DC, Lin CE, Lazow MA, Locke KG, Zhang X, Birch DG. Thickness of receptor and post-receptor retinal layers in patients with retinitis pigmentosa measured with frequency-domain optical coherence tomography. _Invest Ophthalmol Vis Sci_. 2009;50:2328–2336.

25. Wolf-Schnurrbusch UE, Ceklic L, Brinkmann CK, et al. Macular thickness measurements in healthy eyes using six different optical coherence tomography instruments. _Invest Ophthalmol Vis Sci_. 2009;50:3432–3437.

26. Bringmann A, Pannicke T, Grosche J, et al. Müller cells in the healthy and diseased retina. _Prog Retin Eye Res_. 2006;25:397–424.

27. Birnbach CD, Jarvelainen M, Possin DE, Milam AH. Histopathology and immunocytochemistry of the neurosensory retina in fundus flavimaculatus. _Ophthalmology_. 1994;101:1211–1219.

28. Seitz R, Tamm ER. Müller cells and microglia of the mouse eye react throughout the entire retina in response to the procedure of an intravitreal injection. _Adv Exp Med Biol_. 2014;801:347–353.

29. Singh RK, Kolandaivelu S, Ramamurthy DV. Early alteration of retinal neurons in Aipl1−/− animals. _Invest Ophthalmol Vis Sci_. 2014;55:3081–3092

30. Jacobson SG, Cideciyan AV. Treatment possibilities for retinitis pigmentosa. _N Engl J Med_. 2010;363:1669–1671.

31. Francke M, Makarov F, Kacza J, et al. Retinal pigment epithelium melanin granules are phagocytozed by Müller glial cells in experimental retinal detachment. _J Neurocytol_. 2001; 30:131–136.

32. Honjo M, Tanihara H, Kido N, Inatani M, Okazaki K, Honda Y. Expression of ciliary neurotrophic factor activated by retinal Müller cells in eyes with NMDA- and kainic acid-induced neuronal death. _Invest Ophthalmol Vis Sci_. 2000;41:552–560.

33. Oku H, Ikeda T, Honma Y, et al. Gene expression of neurotrophins and their high-affinity Trk receptors in cultured human Müller cells. _Ophthalmic Res_. 2002;34:38–42.

34. Goldberg NR, Greenberg JP, Laud K, Tsang S, Freund KB. Outer retinal tubulation in degenerative retinal disorders. _Retina_. 2013;33:1871–1876.

35. Zweifel SA, Engelbert M, Laud K, Margolis R, Spaide RF, Freund KB. Outer retinal tubulation: a novel optical coherence tomography finding. *Arch Ophthalmol*. 2009;127:1596–1602.

36. Takeda M, Takamiya A, Jiao JW, et al. Alpha-aminoadipate induces progenitor cell properties of Müller glia in adult mice. *Invest Ophthalmol*. 2008;49:1142–1150.

37. Wan J, Zheng H, Chen ZL, Xiao HL, Shen ZJ, Zhou GM. Preferential regeneration of photoreceptor from Müller glia after retinal degeneration in adult rat. *Vision Res*. 2008;48: 223–234.

38. Fujinami K, Sergouniotis PI, Davidson AE, et al. Clinical and molecular analysis of Stargardt disease with preserved foveal structure and function. *Am J Ophthalmol*. 2013;156:487– 501.e1.

39. Westeneng-van Haaften SC, Boon CJ, Cremers FP, Hoefsloot LH, den Hollander AI, Hoyng CB. Clinical and genetic characteristics of late-onset Stargardt's disease. *Ophthalmology*. 2012;119:1199–1210.

40. Curcio CA, Sloan KR, Kalina RE, Hendrickson AE. Human photoreceptor topography. *J Comp Neurol*. 1990;292:497– 523.

41. Saari JC. Vitamin A metabolism in rod and cone visual cycles. *Annu Rev Nutr*. 2012;32:125–145.

42. Hecht S, Haig C, Chase AM. The influence of light adaptation on subsequent dark adaptation of the eye. *J Gen Physiol*. 1937;20:831–850.

43. Imai H, Kefalov V, Sakurai K, et al. Molecular properties of rhodopsin and rod function. *J Biol Chem*. 2007;282:6677– 6684.

44. Lamb TD, Pugh EN Jr. Dark adaptation and the retinoid cycle of vision. *Prog Retin Eye Res*. 2004;23:307–380.

45. Das SR, Bhardwaj N, Kjeldbye H, Gouras P. Muller cells of chicken retina synthesize 11-cis-retinol. *Biochem J*. 1992;285; 907–913.

46. Mata NL, Radu RA, Clemmons RC, Travis GH. Isomerization and oxidation of vitamin A in cone-dominant retinas: a novel pathway for visual-pigment regeneration in daylight. *Neuron*. 2002;36:69–80.

47. Muniz A, Villazana-Espinoza ET, Thackeray B, Tsin AT. 11-cis-Acyl-CoA:retinol O-acyltransferase activity in the primary culture of chicken Muller cells. *Biochemistry*. 2006;45: 12265–12273.

48. Ahmad KM, Klug K, Herr S, Sterling P, Schein S. Cell density ratios in a foveal patch in macaque retina. *Vis Neurosci*. 2003; 20:189–209.

49. Burris C, Klug K, Ngo IT, Sterling P, Schein S. How Müller glial cells in macaque fovea coat and isolate the synaptic terminals of cone photoreceptors. *J Comp Neurol*. 2002;453:100–111.